Stem Cell Reports
Article

ISSCR

OPEN ACCESS

Functional Properties of Engineered Heart Slices Incorporating Human Induced Pluripotent Stem Cell-Derived Cardiomyocytes

Adriana Blazeski,[1] Justin Lowenthal,[1] Renjun Zhu,[1] Jourdan Ewoldt,[1] Kenneth R. Boheler,[1,2,3] and Leslie Tung[1,*]

[1]Department of Biomedical Engineering, The Johns Hopkins University, Baltimore, MD 21205, USA
[2]Stem Cell and Regenerative Medicine Consortium, LKS Faculty of Medicine, Hong Kong University, Hong Kong, SAR
[3]Division of Cardiology, The Johns Hopkins University School of Medicine, Baltimore, MD 21205, USA
*Correspondence: ltung@jhu.edu
https://doi.org/10.1016/j.stemcr.2019.04.002

SUMMARY

Human induced pluripotent stem cell-derived cardiomyocytes (hiPSC-CMs) hold great promise for cardiac studies, but their structural and functional immaturity precludes their use as faithful models of adult myocardium. Here we describe engineered heart slices (EHS), preparations of decellularized porcine myocardium repopulated with hiPSC-CMs that exhibit structural and functional improvements over standard culture. EHS exhibited multicellular, aligned bundles of elongated CMs with organized sarcomeres, positive inotropic responses to isoproterenol, anisotropic conduction of action potentials, and electrophysiological functionality for more than 200 days. We developed a new drug assay, GRIDS, that serves as a "fingerprint" of cardiac drug sensitivity for a range of pacing rates and drug concentrations. GRIDS maps characterized differences in drug sensitivity between EHS and monolayers more clearly than changes in action potential durations or conduction velocities. EHS represent a tissue-like model for long-term culture, structural, and functional improvement, and higher fidelity drug response of hiPSC-CMs.

INTRODUCTION

The advancement in cardiac differentiation strategies for human pluripotent stem cells (hPSCs) (Burridge et al., 2012) has opened up opportunities for new *in vitro* studies of human cardiomyocytes (CMs). However, widespread and reliable use of hPSC-CMs requires the development of preparations that can recapitulate essential features of myocardial structure and function: e.g., elongated CMs in arrays that mimic myofiber bundles, coordinated contraction, fast and uniform conduction of action potentials (APs), and appropriate sensitivity to cardioactive drugs. To this end, a variety of strategies have been employed to make tissue-like constructs, including casting hPSC-CMs in hydrogels (Tzatzalos et al., 2015), seeding them onto synthetic matrices (Ma et al., 2014), and fabricating cell sheets (Matsuura et al., 2012). These efforts have resulted in structurally organized, multicellular preparations that promote more mature states of cardiac gene expression, contraction, calcium handling, and conduction. However, their ultimate usefulness for *in vitro* studies may be hampered by the inability to maintain functionality during long-term culture and the absence of instructive cues typically present in the adult myocardium.

An emerging strategy is to use decellularized myocardial matrix as a source of biochemical, topographical, and biomechanical cues present in the heart to direct differentiation and maturation of PSC-CMs. Decellularized myocardial matrix decreases stem cell pluripotency and induces differentiation in iPSCs (Carvalho et al., 2012) and early cardiac progenitor cells (Lu et al., 2013). The idea that multicomponent extracellular matrix (ECM) can enhance cardiac differentiation has been demonstrated with hydrogels composed of solubilized acellular porcine matrix (Duan et al., 2011) or solubilized basement membrane Matrigel preparations (Zhang et al., 2012). Cell culture coatings made from these solubilized, acellular matrix sources or from decellularized sheets of supporting cells enhance the structural organization of CMs (Baharvand et al., 2005) and temporally advance the expression of cardiac genes and proteins in cardiac progenitor cells (French et al., 2012). Acellular matrix can improve the response of single hiPSC-CMs to cardiac drugs so that they more closely resemble that of adult CMs (Feaster et al., 2015). Although these findings suggest that decellularized matrix may be uniquely suited to guide cellular organization, promote CM lineage commitment, accelerate maturation, and promote better physiological responses to cardiac drugs, reseeding decellularized myocardium with hPSCs and differentiating these cells into a dense tissue-like network of CMs has proven difficult. Furthermore, an important step toward the creation of a truly tissue-like preparation of human CMs would be the demonstration of a high degree of electrophysiological and contractile function in preparations generated on decellularized matrices.

In this study, we have seeded CMs onto thin decellularized slices of ECM (dECM slices) derived from pig heart. Our goal was to create tissue-like constructs that would: support a functional network of hiPSC-CMs, organize and align CMs, exhibit coordinated contraction and uniform

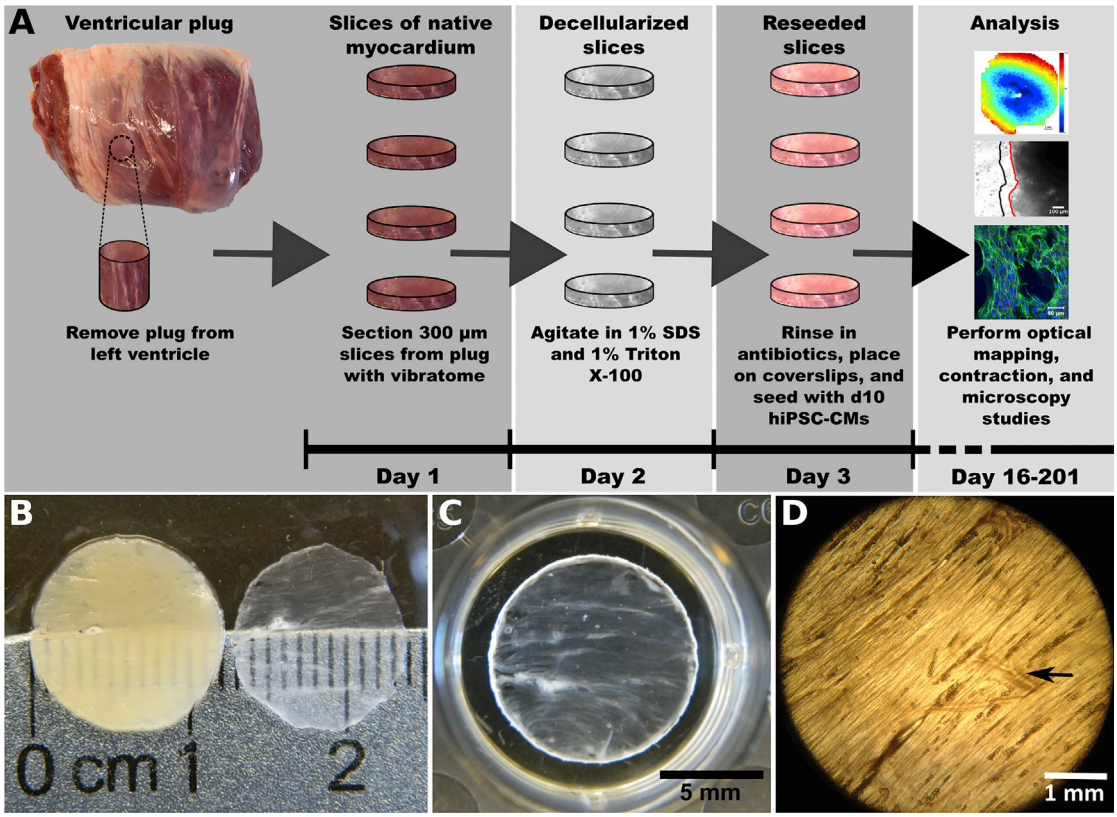

Figure 1. Preparation of EHS

(A) The workflow for preparing slices.

(B) Slices of myocardium before (left) and after decellularization (right).

(C) Slices attached to the edges of a plastic coverslip and placed in the wells of a standard culture dish before cell seeding.

(D) Light micrograph of decellularized slice showing ECM and portion of vasculature (arrow indicates vessel).

See also Figure S1.

AP propagation, maintain functionality during prolonged culture, have a sufficiently large area to support reentrant arrhythmia, and exhibit a robust response to cardiac drugs for a wide range of concentrations and pacing rates. We find that CM-seeded tissues reliably recapitulate key structural, functional and electrophysiological features of native myocardium and proved more sensitive in drug screening assays where electrical pacing could be varied.

RESULTS

Thin Slices of Decellularized Myocardium Promote Growth and Global Alignment of hiPSC-CMs

We sectioned 12-mm diameter plugs of left ventricular myocardium from porcine hearts into 300-µm-thick slices using a vibratome (Figure 1A). Full decellularization was achieved after 3.5 h of exposure to detergents (Figure 1B). The resulting thin dECM slices did not maintain their shape when removed from liquid, a problem that was resolved by spreading each slice onto a plastic coverslip. Under these conditions, the perimeter of the dECM slice could adhere to the edges of the coverslip (Figure 1C). The dECM slice exhibited overall alignment of ECM and residual vasculature (Figure 1D).

We confirmed the removal of cells and nuclei by assaying slices before and after treatment with detergents. Native slices contained an abundance of cells, indicated by nuclear staining and intracellular F-actin (Figure S1A), which were absent in dECM slices (Figure S1E). Decellularization left intact the ECM components of collagen I (Figures S1B and S1F), collagen III (Figures S1C and S1G), and laminin (Figures S1D and S1H). The organization of collagen fibers in the dECM slice, as visualized by second-harmonic generation (SHG) imaging, was not altered by storing sectioned slices at −80°C before decellularization or by storing ventricular plugs at −80°C before slicing and decellularization (Figures S1I–S1L). Overall, each component analyzed in the

dECM slices largely retained the structural alignment observed in native slices. Our decellularization method decreased the DNA content of slices more than 160-fold to approximately 0.12 μg/mg initial dry weight, as reported previously (Blazeski et al., 2015). Taken together, these data suggest that the detergent-treated slices are almost completely devoid of cells and nuclei but retain a mixture of ECM components that remains structurally organized.

Differentiated progeny from hiPSCs were seeded onto the dECM slices at d10–12 (Figure 1A) to form engineered heart slices (EHS). Our cardiac differentiation protocol yielded a mixture of, on average, ~83% cTnT-positive hiPSC-CMs and ~17% cTnT-negative non-CMs (Figures S2A and S2B). After 16 days of EHS culture (d26–28), these cells formed multicellular, aligned tissue layers (Figures 2A and 2B). CM alignment, however, decreased in the apical cell layers farthest from the surface of the matrix (Figure S3). Cells, which organized into multicellular strands, were made up mainly of cardiac troponin I (cTnI)-positive CMs, with vimentin-positive non-CMs located primarily in the center of the strands (Figure 2A). CMs also exhibited striations characteristic of sarcomere structures and stained positively for Cx43 (Figure 2C) localized along the periphery of the cells (Figure S3D). Transmission electron micrographs of hiPSC-CMs on slices showed the presence of z-lines in sarcomeres that were surrounded by mitochondria (Figure 2D).

Comparisons were then made between d55 hiPSC-CMs seeded at low density to make EHS and those on Geltrex-coated cell culture dishes to evaluate the effect of the matrix on cellular shape and organization. CMs grown on Geltrex were cobblestone-like and had randomly oriented sarcomeres (Figure 2E). Age-matched CMs on EHS were elongated, with sarcomeres arranged along the long axis of each cell (Figure 2F). Interestingly, the morphological trait of elongated cells and aligned sarcomeres became ingrained with time on the tissue slices. For example, when hiPSC-CMs were maintained for a prolonged period of time (139 days) as EHS and subsequently dissociated and replated under standard 2D culture systems, the cultivated cells retained an elongated morphology and exhibited highly organized sarcomeres (Figure 2G). Cellular alignment on the dECM slice was assessed by the orientation and elongation ratio (long axis/short axis) of nuclei fitted by ellipses (Figures 2H and 2I). In hiPSC-CMs cultured on Geltrex in standard cell culture dishes, the nuclear elongation ratio was 1.38 ± 1.21 with an SD of 56.6° around the mean angle of orientation (n = 165 nuclei, Figure 2J). The nuclei of CMs cultured as EHS were more elongated and more closely oriented in the same direction, having an elongation ratio of 1.70 ± 1.37 and an SD of 50.1° around the mean angle of orientation (n = 233 nuclei, Figure 2J).

EHS Contract Synchronously and Respond to Isoproterenol

Spontaneous and asynchronous contractions were apparent in EHS within 24 h of cell seeding, but this transitioned to synchronous contractions in about 1 week. At d28 and d74, we evaluated contraction as the change in EHS area in a region where the slice edge was freed from the coverslip. The contracting hiPSC-CMs deformed the ECM, permitting us to monitor the change in area as an approximation of the degree of contraction. When stimulated at a pacing cycle length (PCL) of 666 ms (1.5 Hz, n = 8), the EHS area in the field of view decreased, on average, by 2.0% ± 1.3% from its value at rest (Figures 3A–3C; Video S1). The addition of 1 μM isoproterenol resulted in a 1.5 ± 0.6-fold larger area change, and subsequent washout of the drug brought the area change back down to 1.1 ± 0.4 times the baseline value (Figure 3). Increasing the pacing rate from 1.5 Hz (666 ms PCL) to 2 Hz (500 ms PCL) resulted in an area change of 0.7 ± 0.1 (negative force-frequency relationship) that was statistically significant, whereas decreasing the pacing rate from 1.5 to 1 Hz (1000 ms PCL) resulted in an area change (1.1 ± 0.1) that was not statistically significant (Figure S4B).

EHS Exhibit Anisotropic Electrical Conduction and Retain Functionality during Long-Term Culture

EHS at d54–58 could be pace-captured starting from a PCL of 1000 ms to 425 ± 51 ms (n = 6) and exhibited propagation of APs throughout the entire preparation (Figure 4A; Video S2). Action potential durations (APDs) showed physiological rate dependence: APD_{30} and APD_{80} decreased during incremental increases in pacing rate (incremental decreases in PCL from 1000 to 400 ms, n = 4–6) (Figure 4C; Table S1). Both transverse and longitudinal conduction velocity (CV) showed physiological rate dependence, decreasing with increasing pacing rate (Figure 4D). The resultant CV anisotropy ratio remained relatively constant around 1.4 over the range of PCLs from 500 to 1000 ms (Figure 4E), suggesting that the increases in pacing rate primarily affected sodium channel availability (i.e., excitability) and did not cause significant changes in gap junctional conductance (de Diego et al., 2011).

The high degree of electrophysiological function in EHS was applicable to other hiPSC lines. This was demonstrated through the analyses of EHS made with hiPSC-CMs derived from a patient with confirmed LQT2. LQT2 is a cardiac disorder characterized by prolonged ventricular repolarization arising from mutations in the rapid delayed potassium channel (HERG) that increases the incidence of arrhythmias (Tester and Ackerman, 2014). As with wild-type (WT) EHS, LQT2 EHS cells were aligned and organized into multicellular strands (Figures S5A and S5B), in which non-CMs were in contact with the ECM, while the CMs

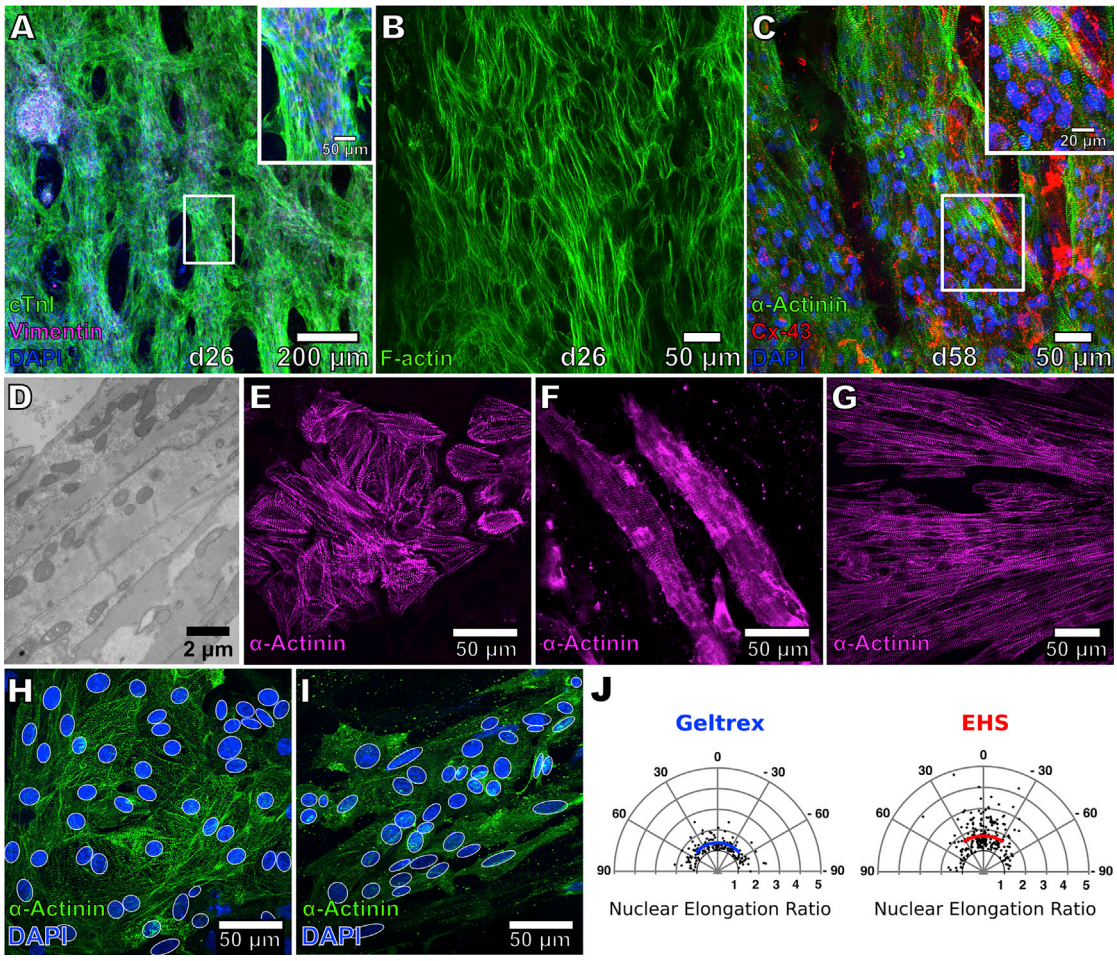

Figure 2. Morphology of hiPSC-CMs on EHS

(A) Immunostaining for cardiac troponin I (green), DAPI (blue), and vimentin (magenta) in EHS. Scale bar, 50 μm (inset).

(B) Staining for F-actin in EHS.

(C) Staining for α-actinin (green) and Cx43 (red) in EHS. Scale bar, 20 μm (inset). Higher-magnification view in the insets correspond to region outlined by white rectangle. hiPSC-CMs were cultured in EHS for either 16 or 48 days (d26 or d58 of differentiation, respectively).

(D) Transmission electron micrograph of hiPSC-CMs in EHS showing myofilaments and mitochondria.

(E and F) Staining for α-actinin in hiPSC-CMs cultured at a low density on Geltrex (E) or on decellularized slices (F).

(G) Staining for α-actinin in hiPSC-CMs seeded on slices at d13, dissociated after prolonged culture (139 days) and replated on Geltrex.

(H and I) DAPI staining of nuclei (blue, delineated by white outline) in hiPSC-CMs (green, α-actinin immunostaining) on Geltrex (H) and on EHS (I).

(J) Analysis of d24 hiPSC-CM nuclear shape and orientation in EHS and on Geltrex. Radial distances of data points reflect elongation ratios (long axis/short axis) of nuclei that were fitted by white ellipses in (H) and (I). Solid blue and red lines indicate mean nuclear elongation ratios for cells on Geltrex (n = 165 nuclei) or in EHS (n = 233 nuclei), respectively, while arc lengths correspond to standard deviation from the mean angle of orientation.

See also Figures S2 and S3.

were organized on top of these cells (Figures S5C and S5D). Like our previous observations in WT EHS, LQT2 EHS exhibited anisotropic propagation of APs throughout the slice (Figure S5E). APDs in LQT2 EHS were prolonged compared with those in WT EHS (Figure S5F), recapitulating the hallmark of LQT (Figure S5G, n = 3 LQT2 EHS and n = 5 WT EHS).

In addition to having structurally elongated and organized CMs (Figure 2G), EHS in long-term culture retained cell-connectivity and paceable, coordinated AP activity. Samples that were maintained in culture for more than 2 months (d62–82) exhibited isotropic propagation of APs, typical of thicker cell layers where cells become more randomly oriented (Figure S3), and had CVs ranging from

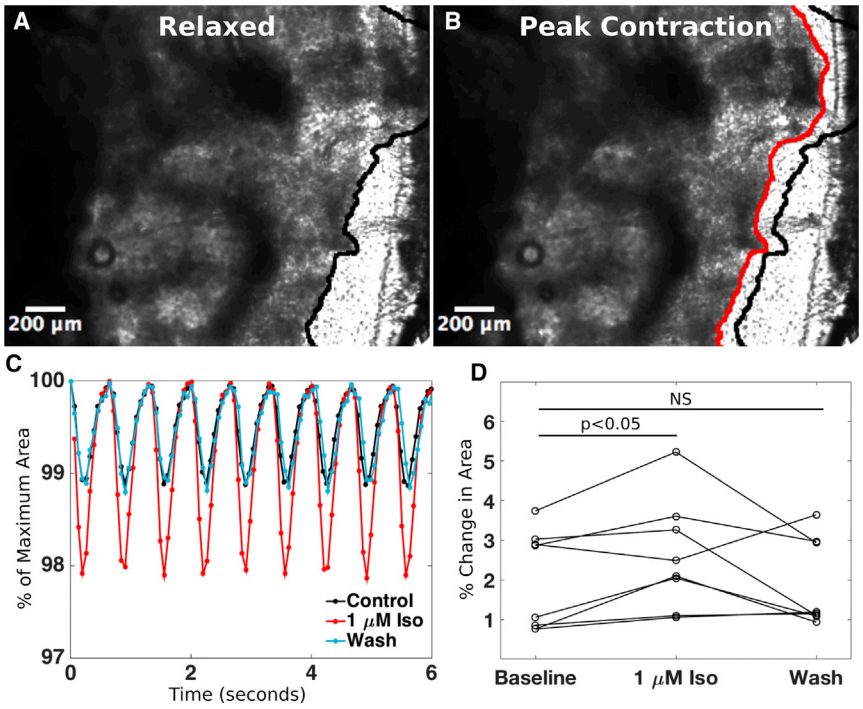

Figure 3. Contraction of EHS and Response to Isoproterenol

(A and B) EHS in relaxed state (A) and at peak contraction (shortening) (B) in response to 666 ms pacing. Black line in (A) and (B) delineates edge of EHS when fully relaxed and red line (B) delineates edge of EHS at maximum contraction.

(C) Percent change in area during contraction (contraction amplitude) in response to pacing at 666 ms normalized to area at rest, plotted at baseline, after the addition of 1 µM isoproterenol, and after washout of the drug.

(D) Percent change in EHS area during isoproterenol and after washout (n = 8 EHS for each group). NS indicates not significantly different from control values.

See also Figure S4 and Video S1.

13.9 ± 1.9 cm/s at 700 ms PCL to 18.4 ± 1.8 cm/s at 1900 ms PCL (Figure 5A; Table S2). The proportion of non-CMs in EHS at d68 increased from that at the time of seeding (Figure S2). EHS using the same batch of cells but cultured for more than 200 days, exhibited lower CVs, which at 1300 and 1500 ms PCL reached statistical significance when compared with d62–82 CVs at the same PCL (Figure 5A; Table S2). Notably, d201 EHS could be paced over a wider range of cycle lengths (CLs), from 2000 ms (now possible because of their lower spontaneous beating rates) to 400 ms (now possible because of their shorter APDs), than that for d62–82 EHS, from 1900 ms PCL to 700 ms. Mean APD_{80} and APD_{30} of d201 EHS were significantly shorter at all PCLs than those of d62–82, respectively (Figure 5C; Table S2), reflecting net increase in inward and/or net decrease in outward AP current in older EHS.

EHS Differ from Standard Monolayer Cultures in their Response to Ion Channel-Modulating Drugs, when Evaluated Using GRIDS Analysis

Based on the improved adult-like cellular morphology, more ventricular-like APs (Figures S6A and S6B) and increased expression levels of numerous ion channel transcripts of hiPSC-CMs after culture on EHS (Figure S6C), we hypothesized that cells on EHS would exhibit differences in drug responses in comparison with standard culture. To test the responsiveness of EHS to ion channel modulators, we developed an assay, called GRIDS (grid of responses indicating drug sensitivity), that characterizes the ability of a cardiac preparation to respond to pacing when exposed to a range of drug concentrations. We used it to compare EHS with age-matched monolayer cultures. APs of EHS and monolayers were evaluated at each drug concentration in the absence of pacing and when subjected to electrical stimulation at PCLs ranging from 2000 to 500 ms. By incorporating a range of pacing rates, GRIDS manifests the distinct sensitivities of different ion currents (Ravens and Wettwer, 1998) and their rate dependencies, and provides a "fingerprint" of drug sensitivity. We observed several types of responses: no spontaneous activity (Figure 6A, i), spontaneously generated APs when no pacing was applied (Figure 6A, ii), extra APs between pacing stimuli (Figure 6A, iii), one AP generated for each pacing stimulus—i.e., 1:1 pace-capture (Figure 6A, iv), and failure to maintain 1:1 pace-capture (lost beats) (Figure 6A, v). We evaluated the effects of each drug on augmenting paced activity by counting the proportion of EHS and monolayers that exhibited extra beats between paced beats ('Fraction With Extra Beats', exemplified in Figure 6A, ii–iii) and on the ability to retain capture by counting the proportion of EHS and monolayers that lost beats during pacing ('Fraction With Lost Beats' exemplified in Figure 6A, v). Further, if application of a drug resulted in spontaneous activity, the EHS or monolayers were counted as having extra beats and included in the 'Fraction With Extra Beats' visualized in the bottom row of each GRIDS analysis.

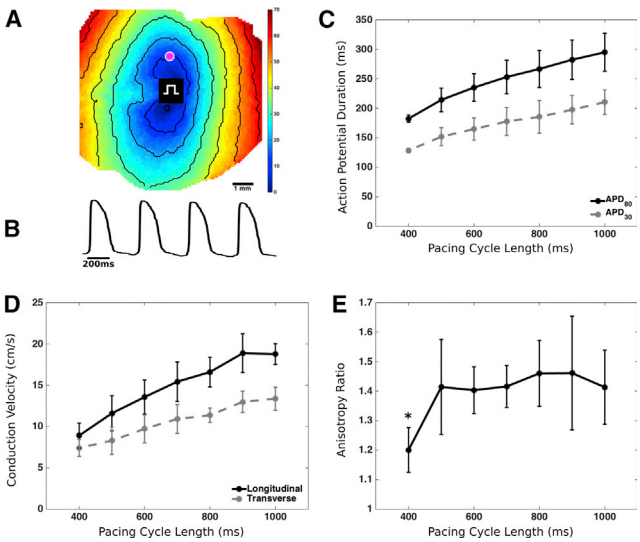

Figure 4. Optical Mapping of EHS

(A) A sample activation map of EHS paced at 500 ms cycle length. Black lines indicate isochrones at 10 ms intervals. Rectangular symbol indicates pacing site.

(B) Sample voltage trace is shown from the site indicated by the magenta point in (A).

(C–E) APD_{30} and APD_{80} as function of pacing cycle length (PCL) (C), CVs in the longitudinal and transverse directions (D), and anisotropy ratios at different pacing rates for d54–58 EHS (E) (n = 4 independent EHS for PCL = 400 ms, and n = 6 independent EHS for PCL >400 ms). *p < 0.05 for difference compared with anisotropy ratio at PCL = 1000 ms. Error bars denote SD.

See also Table S1, Video S2, and Figure S5.

We superfused EHS and monolayers with the rapidly activating potassium current (I_{Kr}) blocker, E-4031, at concentrations ranging from 1 nM to 10 μM (Figure 6A). At increasingly shorter PCLs, a greater fraction of monolayers than EHS lost capture during rapid pacing at concentrations of E-4031 greater than 50 nM, indicating a lower sensitivity of EHS to E-4031 under these conditions. Next, we evaluated the sensitivity of EHS and monolayers to I_{K1} block by superfusing them with $BaCl_2$ (Figure 6B). The spontaneous rate of both EHS and monolayers increased in a concentration-dependent manner (not shown), and this effect was greater in monolayers. At a concentration of 500 μM $BaCl_2$, monolayers were spontaneously beating at rates up to 1 Hz and could be partially pace-captured only at CLs of 1000 ms and less (light blue, yellow, and red squares), while at a concentration of 1 mM nearly all monolayers were spontaneously beating faster than 2 Hz, so only a small fraction could be partially pace-captured at a CL of 500 ms (Figure 6B, bottom, medium blue square). EHS could be overdrive paced at 700 and 1000 ms PCL for all concentrations of $BaCl_2$ (Figure 6B, top). At 1 mM $BaCl_2$, all of the EHS tested lost capture at 500 ms PCL. Taken together, these results suggest that EHS are less sensitive to $BaCl_2$ than monolayers.

We then blocked the slow delayed rectifier K^+ current (I_{Ks}) with chromanol 293B to test its effects on EHS and monolayer cultures (Figure 6C). The fraction of monolayers exhibiting spontaneous activity when no pacing was applied was non-zero and constant at all concentrations except for 5 μM, when it was zero, and 60 μM, when all monolayers exhibited spontaneous activity (Figure 6C, bottom). However, at all concentrations tested, both EHS and monolayers could be pace-captured at all PCLs from 2000 to 500 ms (Figure 6C). Therefore, chromanol 293B had a limited effect on either preparation, suggesting that I_{Ks} is poorly expressed or not functionally active in both monolayers and EHS. Aside from differences in potassium channels, we tested whether L-type calcium channels might also be differentially expressed in EHS and in monolayers, so the channel blocker nifedipine was applied (Figure 6D). As the drug concentration was increased, monolayers lost pace-capture over a wider range of PCL, whereas EHS never lost pace-capture (Figure 6D), indicating that EHS were insensitive to nifedipine in this regard.

In addition to the GRIDS analysis, we evaluated the occurrence of drug-induced prolongations of repolarization, which is an index of liability for acquired long-QT syndrome (Wood and Roden, 2004), as well as conduction slowing, which can be an early sign of conduction block. At a PCL of 1500 ms, E-4031 prolonged APD_{80} (Figure 7A, i–iii) and slowed CV (Figure 7A, iv) in both EHS and monolayers in a concentration-dependent manner over a range of 50 nM to 10 μM. For concentrations up to 150 μM, $BaCl_2$ increased APD_{80} and decreased CV in both preparations in a concentration-dependent manner (Figure 7B), although the decrease in CV reached statistical significance only in EHS. Chromanol 293B (Figure 7C) had no effect on APD_{80} or on CV at concentrations ranging from 1 to 60 μM in either EHS or monolayers. Nifedipine did not affect APD_{80} of EHS and monolayers (not shown), but shortened the plateau phase of the AP in EHS, an effect that was quantified by APD_{30}. At 1500 ms PCL, 0.1 and 0.3 μM nifedipine decreased APD_{30} to a greater extent in EHS than in monolayers (Figure 7D, i–iii), suggesting that EHS have more developed $I_{Ca,L}$ current. Nifedipine does not cause conduction slowing in healthy adult myocardium (Mitchell et al., 1982) and did not significantly decrease CV in our preparations, except at a concentration of 0.01 μM in monolayers (Figure 7D, iv). We further modulated $I_{Ca,L}$ in EHS by applying Bay K 8644, an L-type calcium channel activator, over a range of 0.3 μM–100 μM, and found that it increased APD and decreased CV in a concentration-dependent manner (Figures S7A–S7D). Finally, we found that EHS remained responsive to ion channel-modulating drugs even after long-term culture (d201), as in the case of Bay K

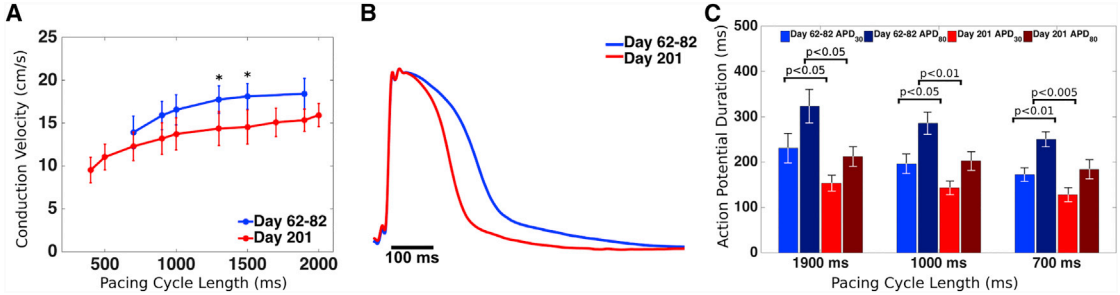

Figure 5. Optical Mapping of EHS after Prolonged Culture

(A) CVs plotted for day 62–82 EHS and day 201 EHS (*p < 0.05 for comparisons between day 62–82 and day 201 at each PCL).

(B) Sample AP traces at 1000 ms PCL in younger and older EHS.

(C) APD_{30} and APD_{80} values at 1900, 1000, and 700 ms PCL for day 62–82 and day 201 EHS. Error bars denote SD. n = 3 independent EHS for day 62–82, and n = 5 independent EHS for day 201.

See also Table S2.

8644 and cromakalim, an activator of the ATP-dependent potassium current ($I_{K,ATP}$) (Figures S7E–S7G).

DISCUSSION

In this study, we repopulated dECM slices with hiPSC-CMs to make EHS with coordinated and syncytial contractile and electrophysiological function. On EHS, reseeded hiPSC-CMs organize in a similar manner to the ordered arrays of fibers found in the native myocardium (Veeraraghavan et al., 2014), becoming elongated and aligned in bundles, with elongated and oriented nuclei, and well-defined, aligned sarcomeres. This is an improvement from the morphology seen in standard cultures, whereby hiPSC-CMs appear more cobblestone-like and have randomly oriented sarcomeres. However, gap junction staining for Cx43 was observed around the periphery of cells in the EHS and does not localize at intercalated discs, reflecting a level of structural immaturity that has also been found in other studies of hPSC-CMs (Zhang et al., 2013). Nevertheless, our EHS are a well-connected and reproducible functional syncytium of CMs that exhibits uniform conduction and coordinated contraction over an area of about 1 cm^2. This overcomes the problem of variable and patchy conduction that occurs in other preparations using decellularized myocardium caused by non-uniform cell seeding (Guyette et al., 2016; Lu et al., 2013; Oberwallner et al., 2015).

The cellular organization of EHS and the resultant anisotropic conduction of APs is guided by the retention of the native oriented matrix in the dECM slice. This strategy to utilize the topographical cues of the ECM differs from those used in other studies to align CMs, including microcontact printing (Wang et al., 2014), hydrogel compaction in the presence of non-myocytes (Liau et al., 2011), and fabricated microgrooved (Rao et al., 2013), nanogrooved (Macadangdang et al., 2015), electrospun (Wanjare et al., 2017), and wrinkled (Wang et al., 2013) substrates. The use of decellularized matrix may confer benefits not present in the other approaches, as there is mounting evidence that the complex chemistry of the matrix can promote stem cell differentiation (Ng et al., 2011) and electrophysiological maturation of CMs (Herron et al., 2016). Our study of EHS demonstrates the suitability of this platform to study electrophysiological function over long-term culture.

Our experimental approach involves the routine production of batches of 10–20 thin tissue slices from ventricular plugs that are subsequently decellularized in parallel. This decellularization method leaves behind a scaffold that retains an organized and aligned structure, made up of multiple ECM components. While various decellularization methods have been developed (Badylak et al., 2011), we chose the method of Ott and colleagues because it preserves non-collagen proteins (particularly, fibrillin, heparin sulfate, and laminin; Guyette et al., 2016), with a trade-off of decreased retention of collagen (Akhyari et al., 2011). These non-collagen components may be particularly beneficial for promoting the differentiation and maintenance of hPSC-CMs (Nakayama et al., 2014). However, because the composition and mechanical properties of the ECM change during development of the heart from the postnatal to adult stage (Gershlak et al., 2013), further work needs to be done to identify the developmental stage that will yield ECM best suited for growth and maintenance of hPSC-CMs. Our method for decellularizing slices is amenable to the use of native myocardium from a variety of sources and can be used to compare the effect of different species, chamber locations, and developmental states of the ECM source on CM electrophysiology and contraction. Automation of the process of anchoring the dECM slice to a

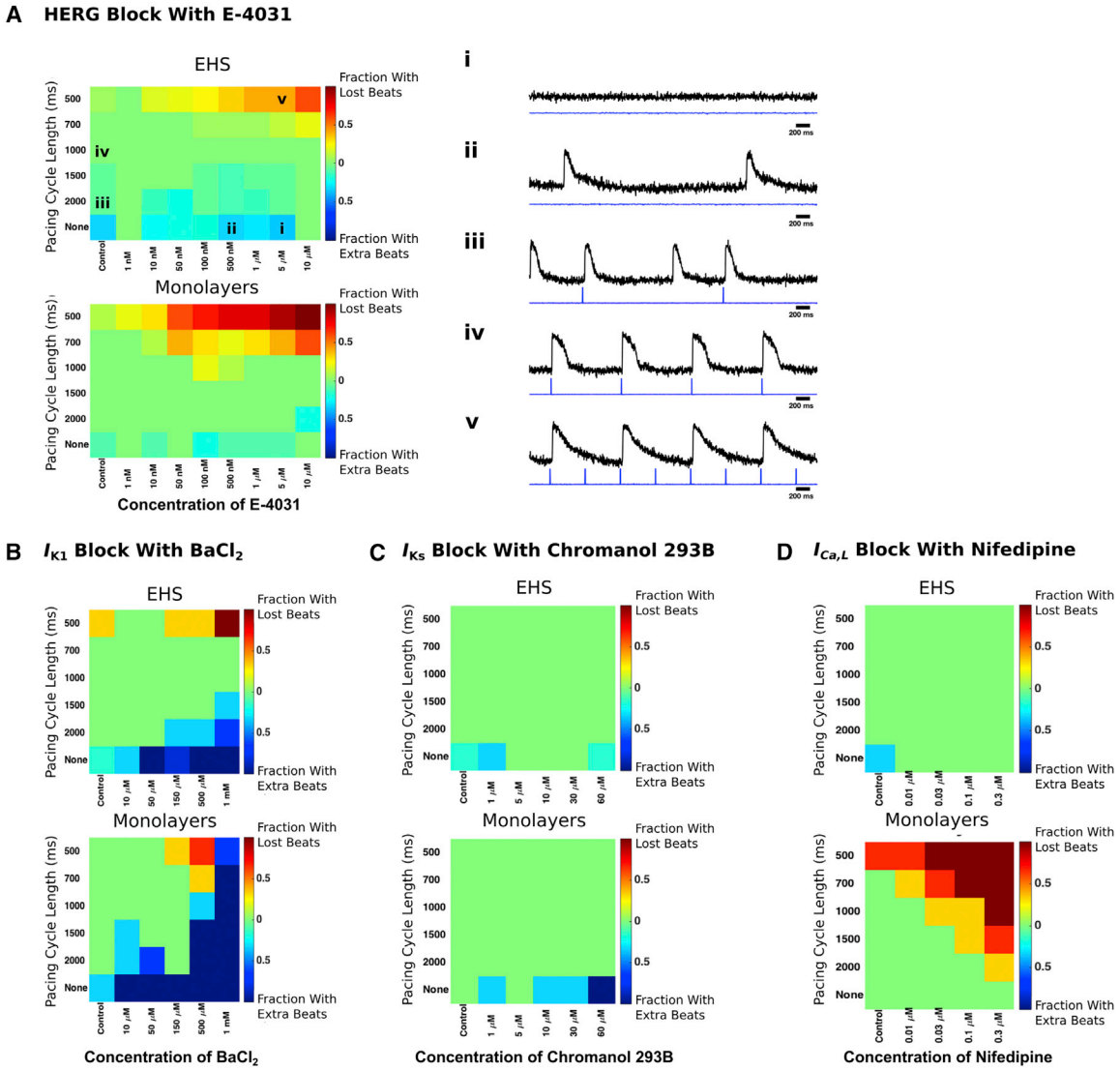

Figure 6. Effect of Cardioactive Drugs on Paced Beats

(A) GRIDS maps of EHS and monolayer responses to E-4031. Sample traces of optical recordings from EHS (right, i–v, top black traces) and corresponding pacing stimuli (right, i–v, bottom blue traces) for examples of: (i) spontaneous activity, (ii) spontaneous activity when no pacing stimuli were applied, (iii) extra beats during pacing, (iv) capture of each paced beat, and (v) lost beats during pacing. PCL and concentration of E-4031 applied during the sample traces is indicated by the squares labeled i–v in the color grid (left). Color bars indicate the fraction of total monolayers or EHS which lost beats illustrated in (v) or gained extra beats illustrated in (iii). n = 5–10 independent EHS and n = 5–18 independent EHS.

(B) GRIDS maps for $BaCl_2$. n = 3 independent monolayers and n = 3–6 independent EHS.

(C) GRIDS maps for chromanol 293B. n = 3 independent monolayers and n = 3–6 independent EHS.

(D) GRIDS maps for nifedipine. n = 3 independent preparations each of monolayers and EHS.

See also Figures S6 and S7.

support will be necessary if large numbers of ECM scaffolds are needed to make EHS for drug discovery and screening.

While EHS exhibited a positive inotropic response to isoproterenol, their fractional shortening (around 2%) was much lower than the 30% fractional shortening reported in adult hearts (Colan et al., 1984), and they also exhibited a negative force-frequency relationship. Further improvements, such as increasingly rapid pacing during culture, can be used to improve contractility and achieve the positive force-frequency relationship found in adult

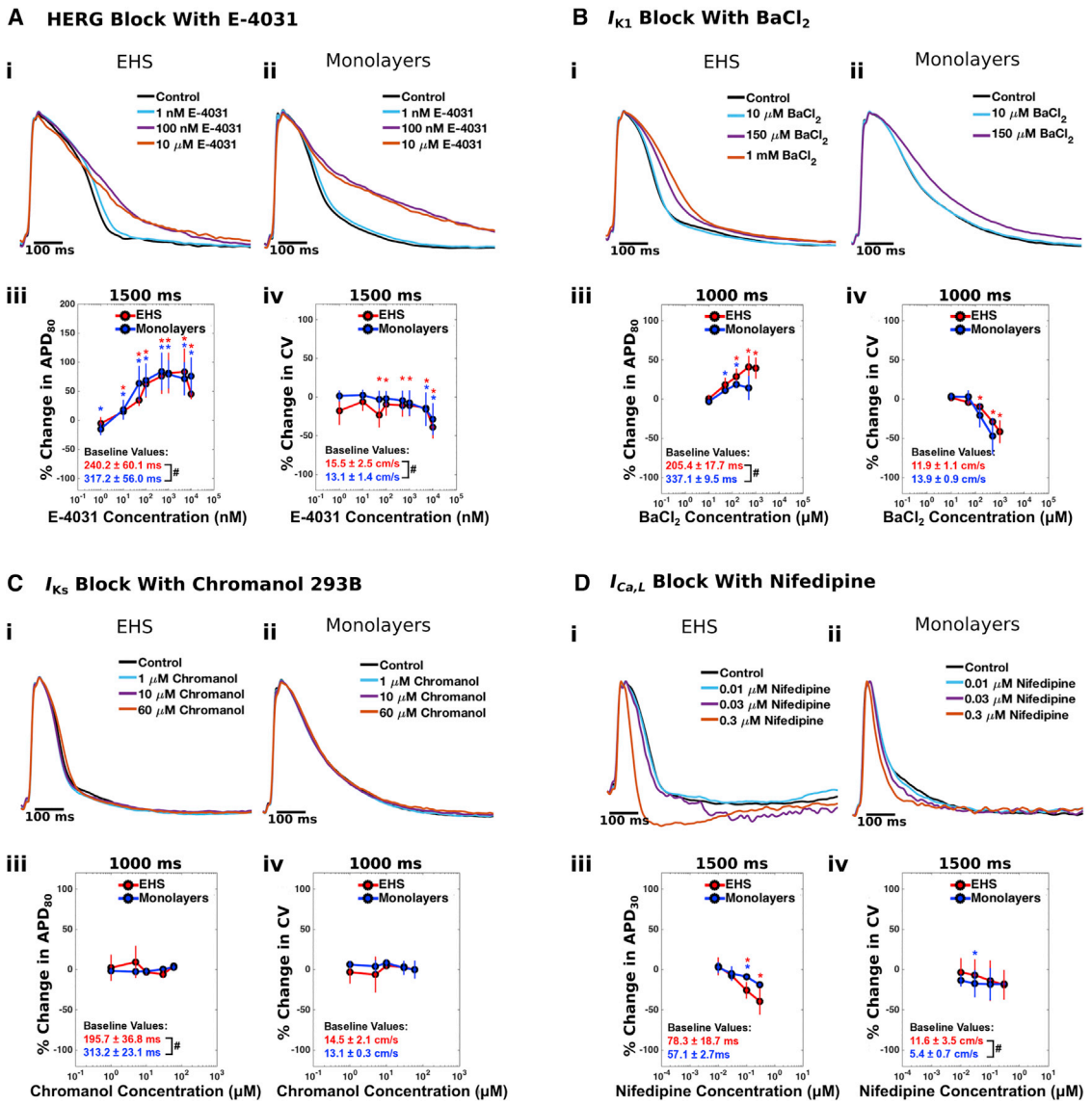

Figure 7. Effect of Cardioactive Drugs on Action Potentials and Conduction Velocities

Action potential recordings from EHS (i) and monolayers (ii) for increasing concentrations of (A) E−4031, (B) $BaCl_2$, (C) chromanol 293B, and (D) nifedipine. Changes in APD_{80} (A–C, iii), APD_{30} (D, iii), and CV (A–D, iv) are plotted for each drug. EHS and monolayers were paced at 1500 ms cycle length for E-4031 and nifedipine and at 1000 ms cycle length for $BaCl_2$ and chromanol 293B. Baseline values of APD and CV before the application of drug are indicated in red for EHS and blue for monolayers in (iii) and (iv) for each drug. Error bars denote standard deviation. Red *, $p < 0.05$ when comparing the percent change for EHS with 0. Blue *, $p < 0.05$ when comparing the percent change for monolayers with 0. #$p < 0.05$ when comparing baseline values for EHS with baseline values for monolayers. n values for EHS and monolayers exposed to each drug are the same as in Figure 6. See also Figure S7.

myocardium (Ronaldson-Bouchard et al., 2018). EHS also exhibited rate-dependent decreases of APD and CV, as well as anisotropic conduction, as is found in the adult human heart (Yue et al., 2005). However, the CV in EHS was less than half of that measured in the adult ventricle (Durrer et al., 1970), and the anisotropy ratio of conduction was substantially less than that in the adult ventricle (Peters and Wit, 1998). The loss of CM alignment in layers of cells farther from the matrix surface likely contributed to a diminished anisotropy ratio.

Amenability to long-term culture is a powerful feature of EHS, because prolonged culture advances the structural organization, cardiac gene expression, and contractile and electrophysiological function of hPSC-CMs (Lundy et al.,

2013). Maintaining multilayers of hiPSC-CMs in standard culture plates for periods of weeks is difficult, because they can detach from the underlying substrate, although individual hiPSC-CMs have been maintained for up to 120 days (Lundy et al., 2013), and multicellular embryoid bodies of hiPSC-CMs have been maintained for up to 360 days (Kamakura et al., 2013). In our study, EHS allowed for stable, long-term culture of a functional syncytium of hiPSC-CMs. Electrophysiological functionality was maintained for more than 200 days—EHS could be pace-captured at PCLs as short as 400 ms, and APs continued to propagate as before throughout the entirety of the preparation, although with some loss of CV that may occur as non-myocytes proliferate over time in EHS culture. Remarkably, hiPSC-CMs cultured long-term within EHS retained their elongated morphology and aligned sarcomeres even after removal from the dECM slice, suggesting that the ECM may have durable effects on cell phenotype. Aside from cues from the ECM, additional steps may be required to optimize the structural organization and function of EHS in long-term culture.

The EHS preparation holds promise for preclinical cardiotoxicity testing, where accurate prediction of arrhythmia risk is essential to remove hazardous drugs from the development pipeline. Currently, drugs are tested for their ability to inhibit HERG and cause QT prolongation, a marker for risk of developing Torsades de Pointes, a tissue-level arrhythmia (Farkas and Nattel, 2010). Most studies of this kind are performed on heterologous expression systems that lack the full complement of cardiac ion channels (Fermini et al., 2016). Such assays also do not account for offsetting mechanisms from non-HERG ion channels that may render a drug safe (Redfern et al., 2003). The EHS preparation addresses these shortcomings as a functional syncytium of human CMs and allows for a multitude of mechanisms by which drugs can affect excitability, including effects on ion currents and electrical coupling.

The GRIDS assay we developed provides a new tool for evaluating drug sensitivity in the context of cellular automaticity and excitability. Changes in spontaneous beating rates are often used to evaluate drug sensitivity of hiPSC-CMs (Gilchrist et al., 2015) and can be altered by drugs that act on $I_{Ca,L}$ or I_{Kr} (Blazeski et al., 2012). However, electrophysiological measurements at variable spontaneous beat rates fail to control for the rate dependence of the various ion currents. On the other hand, GRIDS evaluates the effect of drugs during electrical pacing at different fixed rates. These periodic stimuli introduce controlled, dynamic changes into the system, and the resulting beating patterns are an integrated effect of automaticity, excitability, and refractoriness. The GRIDS map for a given drug is comprised of pace-capture responses across multiple dosing and electrical pacing regimes, and it can serve as a fingerprint of the drug sensitivity. The lowermost row of the GRIDS map reflects the effect of drug on spontaneous rate in the absence of electrical stimulation, while the remaining rows delineate the range of pace-capture across drug dosages. The leftmost column of the map delineates the range of pace-capture under drug-free conditions, while the remaining columns are at different drug dosages. The localization of red blocks in the upper right of the maps for E-4031 and nifedipine (monolayer only) indicates loss of capture of paced beats in the presence of high concentrations of the drug and short PCLs. Localization of blue blocks in the lower right of the maps for $BaCl_2$ indicates a higher fraction of samples with spontaneous activity as drug concentration increased, and the large area of green for chromanol 293B and nifedipine (EHS only) indicates very little response to the drug. Further, across the four drugs tested, in the GRIDS maps the regions of red or blue blocks tended to be smaller, and the region of green tended to be larger, for EHS than for monolayers, revealing that EHS are comparatively less sensitive to these drugs when evaluated for effects on their excitability and ability to capture during pacing. This suggests that EHS express relatively more of the repolarizing currents I_{Kr} and I_{K1}, which are responsible for maintaining the resting potential in adult ventricular cells (Doss et al., 2012), than monolayers. On the other hand, the absence of a chromanol 293B effect supports the notion that both EHS and monolayers have low levels of I_{Ks}, as has been previously described for hPSC-CMs (Ma et al., 2011). The GRIDS maps also indicate that EHS remain excitable at all PCLs and concentrations of nifedipine, whereas monolayers are unable to be pace-captured for every beat for some combinations of PCL and nifedipine concentrations. Increased $I_{Ca,L}$ in EHS would explain why, for the same level of $I_{Ca,L}$ block at a given concentration of nifedipine, EHS would retain enough residual $I_{Ca,L}$ to remain excitable while monolayers would not. Alternatively, the excitability of EHS may be governed more by I_{Na} than by $I_{Ca,L}$ (as in more mature ventricular tissue) compared with that of monolayers (either due to differences in ion channels or because hiPSC-CMs in EHS are less depolarized), so that block of $I_{Ca,L}$ does not decrease excitability.

Our GRIDS maps were able to differentiate the responses of EHS and monolayers to the panel of drugs tested even though measurements of a single electrophysiological parameter, APD prolongation, did not provide a clear snapshot of relative drug sensitivity. In both EHS and monolayers, E-4031 and $BaCl_2$ prolonged APD, chromanol 293B did not change APD, and nifedipine shortened APD. Further, we did not detect differences in drug responses between EHS and monolayers with respect to APD for E-4031(Figure 7A, i–iii) and chromanol 293B (Figure 7C, i–iii), but we did detect them for high

concentrations of $BaCl_2$ (Figure 7B, i–iii) and nifedipine (Figure 7D, i–iii). One limitation of the GRIDS assay is the spontaneous rate of the cells, which dictates the lower bound on the pacing rates that can be applied.

Differences in drug responses of EHS, which tend to be less sensitive but more robust in their ability to be electrically paced over a wider range of rates and drug concentrations when compared with monolayers, can be attributed to a variety of factors. One possibility is that cells in EHS are a more densely packed, thicker syncytium that experiences a lower effective drug concentration than cells in monolayers where diffusion is not limited. Also, differences in the mechanical and biochemical environment in EHS compared with monolayers can result in differences in cell phenotype and AP morphology seen in EHS (more elongated cells with organized sarcomeres), which can affect drug responses. In addition, EHS experience an increase in non-myocytes over time, and this modulation of cell-cell interactions in the preparation could also affect drug responses. Multicellular preparations with large areas, such as EHS, will be needed in future studies to assess the risk for reentrant arrhythmias, which require room for circuitous wavefront propagation to occur. Further, EHS are tissue-like models that can be used in studies aimed at treatment discovery and at creating clinically relevant disease models.

Conclusion

EHS take advantage of the complex biochemical and structural cues of the myocardial ECM to guide the alignment of CMs. Seeded hiPSC-CMs organize as multicellular, anisotropic bundles that contract the EHS and propagate APs uniformly throughout the preparation. EHS can be used for long-term culture of hiPSC-CMs to interrogate processes of cell maturation and response to drugs over time. Drug sensitivity can be evaluated for a range of concentrations and under different pacing rates using the GRIDS assay, which has revealed differences in drug sensitivity between EHS and cell monolayers. In conclusion, EHS are tissue-like models that can be used in long-term electrophysiology and drug studies.

EXPERIMENTAL PROCEDURES

An extended description of the methods can be found in the Supplemental Information.

Preparation of EHS

Slices of porcine myocardium 12 mm in diameter and 300 μm in thickness were sectioned and decellularized as described previously (Blazeski et al., 2015). The dECM slices were spread on plastic 12-mm-diameter coverslips, with the perimeter of each slice wrapped around the edges of the coverslip. Coverslips with slices were placed in wells of standard 24-well culture plates and kept in PBS with antibiotics for up to 2 weeks before reseeding.

hiPSC Differentiation and Culture

WT and LQT2 hiPSC lines with a heterozygous A422T mutation in the potassium voltage-gated, subfamily H, member 2 channel (KCNH2), which is commonly referred to as the HERG channel (Spencer et al., 2014) were gifts from Dr. Bruce Conklin. Both hiPSC lines were differentiated using a monolayer-based protocol (Boheler et al., 2014; Wang et al., 2015). The age of the EHS (d26–d201) is given as the time in days from the start of hiPSC-CM differentiation (d0). On d9, the medium was switched to RPMI 1640 containing B-27 with insulin, and this medium was used for the remainder of time both before and after seeding on the dECM slices.

On d10–12, hiPSC-CM monolayers were dissociated using 0.05% trypsin-EDTA and plated on dECM slices affixed to coverslips at a density of 0.8–1.3 million cells/cm^2. EHS were maintained in culture for 16–191 days before evaluation by optical mapping or contraction measurements.

Imaging of ECM and EHS

Standard fixation and immunostaining techniques were applied to slices before and after decellularization to label F-actin, nuclei, collagen I, collagen III, and laminin. Unstained dECM slices were also imaged by SHG. EHS were fixed and stained using standard techniques for cTnI, α-actinin, connexin 43 (Cx43), vimentin, filamentous actin (F-actin), and nuclei (DAPI). All samples were imaged by confocal microscopy. Nuclear elongation and orientation were analyzed in confocal images of EHS and monolayers using custom MATLAB scripts. Cellular structures in EHS were imaged by transmission electron microscopy.

Contraction Measurements

WT d24–78 EHS were placed in a 35-mm tissue culture dish filled with Tyrode's solution and maintained at 31°C ± 0.1°C for the duration of the experiment. A section of each EHS was detached from the edge of the coverslip so that it could move freely. Each EHS was paced at 1, 1.5, and 2 Hz while the free region was imaged with a CCD camera. A custom MATLAB script was used to segment the image and calculate the change in EHS area over time, which was used as a measure of contraction.

Electrophysiological Studies

Each EHS was placed in Tyrode's solution and stained with 10 μM di-4-ANEPPS for 10 min at 37°C. The EHS was rinsed several times in a dish with warm Tyrode's solution, and then immersed in Tyrode's solution containing 10 μM blebbistatin to suppress contraction. The dish was placed on a 37°C heated stage for the duration of the experiment. At least 5 min after adding blebbistatin, the EHS was stimulated with a point electrode and optically mapped using a CMOS camera (MiCAM Ultima-L, SciMedia). The EHS was paced by 5 ms monophasic rectangular pulses at stepwise increasing rates starting at 0.5 Hz. For some samples, E-4031, chromanol 293B, nifedipine, Bay K 8644, $BaCl_2$, or cromakalim were added for 7 min before mapping. Mapping data were analyzed using custom MATLAB scripts (details provided in

Supplemental Information). APDs at 30% and 80% repolarization (APD_{30} and APD_{80}) were calculated from the optical voltage signal. For drug studies, APD and CV measurements at each concentration were plotted as a percentage of APD and CV measured at baseline, with no drug present.

Statistics

All data are presented as mean ± SD. A Wilcoxon rank-sum test was used to determine statistical significance between control and drug groups for WT EHS contraction experiments, and between WT and LQT2 EHS. Paired, unequal variance, two-tailed t tests were used for statistical tests of significance between experimental groups in all other drug studies, and unpaired, unequal variance, two-tailed t tests were performed to determine the statistical significance between experimental measurements of d62–82 and d201 EHS. Differences were considered statistically significant at $p < 0.05$.

SUPPLEMENTAL INFORMATION

Supplemental Information can be found online at https://doi.org/10.1016/j.stemcr.2019.04.002.

AUTHOR CONTRIBUTIONS

A.B. and L.T. designed the experiments, reviewed and interpreted the data, and wrote the manuscript. A.B. and R.Z. performed cell culture and differentiation under the guidance of K.R.B. J.L. performed the flow cytometry analysis. J.E. performed the slice orientation analysis. A.B. collected and analyzed the rest of the data. All authors edited the manuscript.

ACKNOWLEDGMENTS

This work was supported by Maryland Stem Cell Research Fund grant 2013-MSCRF-II-0045 (to L.T.) and 2016-MSCRF-I-2735 (PIs Gordon Tomaselli and L.T.), NIH grants S10 RR025544 and R01 HL120959 (to L.T.), a Mid-Atlantic AHA predoctoral fellowship (to A.B.), and a Maryland Stem Cell Research postdoctoral fellowship (to A.B.).

Received: January 18, 2017
Revised: April 2, 2019
Accepted: April 2, 2019
Published: May 2, 2019

REFERENCES

Akhyari, P., Aubin, H., Gwanmesia, P., Barth, M., Hoffmann, S., Huelsmann, J., Preuss, K., and Lichtenberg, A. (2011). The quest for an optimized protocol for whole-heart decellularization: a comparison of three popular and a novel decellularization technique and their diverse effects on crucial extracellular matrix qualities. Tissue Eng. Part C Methods *17*, 915–926.

Badylak, S.F., Taylor, D., and Uygun, K. (2011). Whole-organ tissue engineering: decellularization and recellularization of three-dimensional matrix scaffolds. Annu. Rev. Biomed. Eng. *13*, 27–53.

Baharvand, H., Azarnia, M., Parivar, K., and Ashtiani, S.K. (2005). The effect of extracellular matrix on embryonic stem cell-derived cardiomyocytes. J. Mol. Cell. Cardiol. *38*, 495–503.

Blazeski, A., Zhu, R., Hunter, D.W., Weinberg, S.H., Zambidis, E.T., and Tung, L. (2012). Cardiomyocytes derived from human induced pluripotent stem cells as models for normal and diseased cardiac electrophysiology and contractility. Prog. Biophys. Mol. Biol. *110*, 166–177.

Blazeski, A., Kostecki, G.M., and Tung, L. (2015). Engineered heart slices for electrophysiological and contractile studies. Biomaterials *55*, 119–128.

Boheler, K.R., Bhattacharya, S., Kropp, E.M., Chuppa, S., Riordon, D.R., Bausch-Fluck, D., Burridge, P.W., Wu, J.C., Wersto, R.P., Chan, G.C.F., et al. (2014). A human pluripotent stem cell surface N-glycoproteome resource reveals markers, extracellular epitopes, and drug targets. Stem Cell Reports *3*, 185–203.

Burridge, P.W., Keller, G., Gold, J.D., and Wu, J.C. (2012). Production of de novo cardiomyocytes: human pluripotent stem cell differentiation and direct reprogramming. Cell Stem Cell *10*, 16–28.

Carvalho, J.L., de Carvalho, P.H., Gomes, D.A., and Goes, A.M. (2012). Characterization of decellularized heart matrices as biomaterials for regular and whole organ tissue engineering and initial in-vitro recellularization with ips cells. J. Tissue Sci. Eng. (*Suppl 11*), 002.

Colan, S.D., Borow, K.M., and Neumann, A. (1984). Left ventricular end-systolic wall stress-velocity of fiber shortening relation: a load-independent index of myocardial contractility. J. Am. Coll. Cardiol. *4*, 715–724.

de Diego, C., Chen, F., Xie, Y., Pai, R.K., Slavin, L., Parker, J., Lamp, S.T., Qu, Z., Weiss, J.N., and Valderrábano, M. (2011). Anisotropic conduction block and reentry in neonatal rat ventricular myocyte monolayers. Am. J. Physiol. Heart Circ. Physiol. *300*, H271–H278.

Doss, M.X., Di Diego, J.M., Goodrow, R.J., Wu, Y., Cordeiro, J.M., Nesterenko, V.V., Barajas-Martínez, H., Hu, D., Urrutia, J., Desai, M., et al. (2012). Maximum diastolic potential of human induced pluripotent stem cell-derived cardiomyocytes depends critically on I_{Kr}. PLoS One *7*, e40288.

Duan, Y., Liu, Z., O'Neill, J., Wan, L.Q., Freytes, D.O., and Vunjak-Novakovic, G. (2011). Hybrid gel composed of native heart matrix and collagen induces cardiac differentiation of human embryonic stem cells without supplemental growth factors. J. Cardiovasc. Transl. Res. *4*, 605–615.

Durrer, D., van Dam, R.T., Freud, G.E., Janse, M.J., Meijler, F.L., and Arzbaecher, R.C. (1970). Total excitation of the isolated human heart. Circulation *41*, 899–912.

Farkas, A.S., and Nattel, S. (2010). Minimizing repolarization-related proarrhythmic risk in drug development and clinical practice. Drugs *70*, 573–603.

Feaster, T.K., Cadar, A.G., Wang, L., Williams, C.H., Chun, Y.W., Hempel, J.E., Bloodworth, N., Merryman, W.D., Lim, C.C., Wu, J.C., et al. (2015). Matrigel mattress: a method for the generation of single contracting human-induced pluripotent stem cell-derived cardiomyocytes. Circ. Res. *117*, 995–1000.

Fermini, B., Hancox, J.C., Abi-Gerges, N., Bridgland-Taylor, M., Chaudhary, K.W., Colatsky, T., Correll, K., Crumb, W., Damiano,

B., Erdemli, G., et al. (2016). A new perspective in the field of cardiac safety testing through the comprehensive in vitro proarrhythmia assay paradigm. J. Biomol. Screen. *21*, 1–11.

French, K.M., Boopathy, A.V., DeQuach, J.A., Chingozha, L., Lu, H., Christman, K.L., and Davis, M.E. (2012). A naturally derived cardiac extracellular matrix enhances cardiac progenitor cell behavior in vitro. Acta Biomater. *8*, 4357–4364.

Gershlak, J.R., Resnikoff, J.I.N., Sullivan, K.E., Williams, C., Wang, R.M., and Black, L.D. (2013). Mesenchymal stem cells ability to generate traction stress in response to substrate stiffness is modulated by the changing extracellular matrix composition of the heart during development. Biochem. Biophys. Res. Commun. *439*, 161–166.

Gilchrist, K.H., Lewis, G.F., Gay, E.A., Sellgren, K.L., and Grego, S. (2015). High-throughput cardiac safety evaluation and multiparameter arrhythmia profiling of cardiomyocytes using microelectrode arrays. Toxicol. Appl. Pharmacol. *288*, 249–257.

Guyette, J.P., Charest, J.M., Mills, R.W., Jank, B.J., Moser, P.T., Gilpin, S.E., Gershlak, J.R., Okamoto, T., Gonzalez, G., Milan, D.J., et al. (2016). Bioengineering human myocardium on native extracellular matrix. Circ. Res. *118*, 56–72.

Herron, T.J., Da Rocha, A.M., Campbell, K.F., Ponce-Balbuena, D., Willis, B.C., Guerrero-Serna, G., Liu, Q., Klos, M., Musa, H., Zarzoso, M., et al. (2016). Extracellular matrix-mediated maturation of human pluripotent stem cell-derived cardiac monolayer structure and electrophysiological function. Circ. Arrhythm. Electrophysiol. *9*, 1–12.

Kamakura, T., Makiyama, T., Sasaki, K., Yoshida, Y., Wuriyanghai, Y., Chen, J., Hattori, T., Ohno, S., Kita, T., Horie, M., et al. (2013). Ultrastructural maturation of human-induced pluripotent stem cell-derived cardiomyocytes in a long-term culture. Circ. J. *77*, 1307–1314.

Liau, B., Christoforou, N., Leong, K.W., and Bursac, N. (2011). Pluripotent stem cell-derived cardiac tissue patch with advanced structure and function. Biomaterials *32*, 9180–9187.

Lu, T.-Y., Lin, B., Kim, J., Sullivan, M., Tobita, K., Salama, G., and Yang, L. (2013). Repopulation of decellularized mouse heart with human induced pluripotent stem cell-derived cardiovascular progenitor cells. Nat. Commun. *4*, 2307.

Lundy, S.D., Zhu, W.-Z., Regnier, M., and Laflamme, M.A. (2013). Structural and functional maturation of cardiomyocytes derived from human pluripotent stem cells. Stem Cells Dev. *22*, 1991–2002.

Ma, J., Guo, L., Fiene, S.J., Anson, B.D., Thomson, J.A., Kamp, T.J., Kolaja, K.L., Swanson, B.J., and January, C.T. (2011). High purity human-induced pluripotent stem cell-derived cardiomyocytes: electrophysiological properties of action potentials and ionic currents. Am. J. Physiol. Heart Circ. Physiol. *301*, H2006–H2017.

Ma, Z., Koo, S., Finnegan, M.A., Loskill, P., Huebsch, N., Marks, N.C., Conklin, B.R., Grigoropoulos, C.P., and Healy, K.E. (2014). Three-dimensional filamentous human diseased cardiac tissue model. Biomaterials *35*, 1367–1377.

Macadangdang, J., Guan, X., Smith, A.S.T., Lucero, R., Czerniecki, S., Childers, M.K., Mack, D.L., and Kim, D.-H. (2015). Nanopatterned human iPSC-based model of a dystrophin-null cardiomyopathic phenotype. Cell. Mol. Bioeng. *8*, 320–332.

Matsuura, K., Wada, M., Shimizu, T., Haraguchi, Y., Sato, F., Sugiyama, K., Konishi, K., Shiba, Y., Ichikawa, H., Tachibana, A., et al. (2012). Creation of human cardiac cell sheets using pluripotent stem cells. Biochem. Biophys. Res. Commun. *425*, 321–327.

Mitchell, L.B., Schroeder, J.S., and Mason, J.W. (1982). Comparative clinical electrophysiologic effects of diltiazem, verapamil and nifedipine: a review. Am. J. Cardiol. *49*, 629–635.

Nakayama, K.H., Hou, L., and Huang, N.F. (2014). Role of extracellular matrix signaling cues in modulating cell fate commitment for cardiovascular tissue engineering. Adv. Healthc. Mater. *3*, 628–641.

Ng, S.L.J., Narayanan, K., Gao, S., and Wan, A.C.A. (2011). Lineage restricted progenitors for the repopulation of decellularized heart. Biomaterials *32*, 7571–7580.

Oberwallner, B., Brodarac, A., Anić, P., Šarić, T., Wassilew, K., Neef, K., Choi, Y.-H., and Stamm, C. (2015). Human cardiac extracellular matrix supports myocardial lineage commitment of pluripotent stem cells. Eur. J. Cardiothorac. Surg. *47*, 416–425.

Peters, N.S., and Wit, A.L. (1998). Myocardial architecture and ventricular arrhythmogenesis. Circulation *97*, 1746–1754.

Rao, C., Prodromakis, T., Kolker, L., Chaudhry, U.A.R., Trantidou, T., Sridhar, A., Weekes, C., Camelliti, P., Harding, S.E., Darzi, A., et al. (2013). The effect of microgrooved culture substrates on calcium cycling of cardiac myocytes derived from human induced pluripotent stem cells. Biomaterials *34*, 2399–2411.

Ravens, U., and Wettwer, E. (1998). Electrophysiological aspects of changes in heart rate. Basic Res. Cardiol. *93* (*Suppl 1*), 60–65.

Redfern, W.S., Carlsson, L., Davis, A.S., Lynch, W.G., MacKenzie, I., Palethorpe, S., Siegl, P.K.S., Strang, I., Sullivan, A.T., Wallis, R., et al. (2003). Relationships between preclinical cardiac electrophysiology, clinical QT interval prolongation and torsade de pointes for a broad range of drugs: evidence for a provisional safety margin in drug development. Cardiovasc. Res. *58*, 32–45.

Ronaldson-Bouchard, K., Ma, S.P., Yeager, K., Chen, T., Song, L., Sirabella, D., Morikawa, K., Teles, D., Yazawa, M., and Vunjak-Novakovic, G. (2018). Advanced maturation of human cardiac tissue grown from pluripotent stem cells. Nature *556*, 239–243.

Spencer, C.I., Baba, S., Nakamura, K., Hua, E.A., Sears, M.A.F., Fu, C.-C., Zhang, J., Balijepalli, S., Tomoda, K., Hayashi, Y., et al. (2014). Calcium transients closely reflect prolonged action potentials in iPSC models of inherited cardiac arrhythmia. Stem Cell Reports *3*, 269–281.

Tester, D.J., and Ackerman, M.J. (2014). Genetics of long QT syndrome. Methodist Debakey Cardiovasc. J. *10*, 29–33.

Tzatzalos, E., Abilez, O.J., Shukla, P., and Wu, J.C. (2015). Engineered heart tissues and induced pluripotent stem cells: macro- and microstructures for disease modeling, drug screening, and translational studies. Adv. Drug Deliv. Rev. *96*, 234–244.

Veeraraghavan, R., Gourdie, R.G., and Poelzing, S. (2014). Mechanisms of cardiac conduction: a history of revisions. Am. J. Physiol. Heart Circ. Physiol. *306*, H619–H627.

Wang, G., McCain, M.L., Yang, L., He, A., Pasqualini, F.S., Agarwal, A., Yuan, H., Jiang, D., Zhang, D., Zangi, L., et al. (2014). Modeling the mitochondrial cardiomyopathy of Barth syndrome with induced pluripotent stem cell and heart-on-chip technologies. Nat. Med. *20*, 616–623.

Wang, J., Chen, A., Lieu, D.K., Karakikes, I., Chen, G., Keung, W., Chan, C.W., Hajjar, R.J., Costa, K.D., Khine, M., et al. (2013). Effect of engineered anisotropy on the susceptibility of human pluripotent stem cell-derived ventricular cardiomyocytes to arrhythmias. Biomaterials *34*, 8878–8886.

Wang, Y., Li, Z.C., Zhang, P., Poon, E., Kong, C.W., Boheler, K.R., Huang, Y., Li, R.A., and Yao, X. (2015). Nitric oxide-cGMP-PKG pathway acts on orai1 to inhibit the hypertrophy of human embryonic stem cell-derived cardiomyocytes. Stem Cells *33*, 2973–2984.

Wanjare, M., Hou, L., Nakayama, K.H., Kim, J.J., Mezak, N.P., Abilez, O.J., Tzatzalos, E., Wu, J.C., and Huang, N.F. (2017). Anisotropic microfibrous scaffolds enhance the organization and function of cardiomyocytes derived from induced pluripotent stem cells. Biomater. Sci. *5*, 1567–1578.

Wood, A.J.J., and Roden, D.M. (2004). Drug-induced prolongation of the QT interval. N. Engl. J. Med. *350*, 1013–1022.

Yue, A.M., Franz, M.R., Roberts, P.R., and Morgan, J.M. (2005). Global endocardial electrical restitution in human right and left ventricles determined by noncontact mapping. J. Am. Coll. Cardiol. *46*, 1067–1075.

Zhang, D., Shadrin, I.Y., Lam, J., Xian, H.Q., Snodgrass, H.R., and Bursac, N. (2013). Tissue-engineered cardiac patch for advanced functional maturation of human ESC-derived cardiomyocytes. Biomaterials *34*, 5813–5820.

Zhang, J., Klos, M., Wilson, G.F., Herman, A.M., Lian, X., Raval, K.K., Barron, M.R., Hou, L., Soerens, A.G., Yu, J., et al. (2012). Extracellular matrix promotes highly efficient cardiac differentiation of human pluripotent stem cells: the matrix sandwich method. Circ. Res. *111*, 1125–1136.